Preparation of $MoSi_2$-modified HfB_2-SiC ultra high temperature ceramic anti-oxidation coatings by liquid phase sintering

REN Xuan-ru, WANG Wei-guang, SUN Ke, HU Yu-wen, XU Lei-hua*, FENG Pei-zhong

(*China University of Mining and Technology*, *Xuzhou* 221116, *China*)

Abstract: Liquid-phase sintering combining an in-situ reaction method with a slurry method was used to prepare HfB_2-$MoSi_2$-SiC coatings of controllable composition and thickness. The effect of the $MoSi_2$ content on the oxidation protection of HfB_2-$MoSi_2$-SiC composite coatings in a dynamic aerobic environment from room temperature to 1 500 °C and a static constant temperature at 1 500 °C in air was investigated. The relative oxygen permeability was used to characterize the oxidation resistance of the coatings. The results of dynamic oxidation test at room temperature ~ 1 500 °C show that the initial oxidation weight loss temperature of the samples is increased from 775 to 821 °C, and the maximum weight loss rate is decreased from 0.9×10^{-3} to 0.2×10^{-3} mg·cm^{-2}·s^{-1} with increasing $MoSi_2$ content, the lowest relative oxygen permeability is reduced to 12.2% with the weight loss of the sample being decreased from 1.8% to 0.21%. The mechanism of $MoSi_2$ improving the oxidation protection of the coatings is revealed. With an increase of the $MoSi_2$ content, the amount of SiO_2 glass phase in the coating is increased, and the dispersion of Hf-oxide on the surface is improved so that a Hf-Si-O glass layer with high stability is formed and the weight loss of the sample is reduced from 0.46% to 0.08% after 200 h oxidation at 1 500 °C in air.

Key words: $MoSi_2$; Coating; Oxidation resistance; Multiphase glass layer

1 Introduction

Carbon structural materials, such as graphite and C/C composite materials, are widely used in aerospace and manufacturing industries due to their good physical and mechanical properties such as low density, high specific strength and specific modulus[1–4]. Carbon structural materials are considered as ideal ultra-high-temperature thermal structural materials due to their high melting point (>3 500 °C), unique structural stability, excellent thermal stability and conductivity, low coefficient of thermal expansion, good corrosion resistance and wear resistance[5–11]. While the carbon structural materials are easily oxidized above 400 °C, which affects the thermal structure stability under high temperature and limits their applications[12,13]. Therefore, with the increasing applications of carbon structural materials, improving their oxidation resistance in a wide temperature range to meet the requirements is very important. Based on a large number of experimental and theoretical simulation results, using oxidation protection coating to prevent the oxidation corrosion of carbon materials is the most effective way[14–17].

In recent years, among many anti-oxidation ceramics, the ultra high temperature ceramic HfB_2-SiC composite coating has attracted great attention. The HfB_2 component has super high melting point (3 250 °C), high hardness, high strength and good oxidation resistance[18–22]. Carbon structure materials have good compatibility and coefficient matching of thermal expansion with SiC, which can improve the oxidation resistance of materials by forming a self-healing silicate glass protective layer in aerobic environment. Wang et al.[23] prepared a HfB_2-SiC coating by in-situ reaction. The weight loss rate of the sample after static constant temperature oxidation at 1 500 °C for 753 h is only 0.48%. Jiang et al.[24] prepared a new double layer HfB_2-SiC-Si/SiC-Si coating by combining a slurry method and a gas phase silicon permeation method. After oxidation at 1 600 °C for 230 h, the weight of the samples increased by 0.34%. After oxidation at 900 and 1 500 °C for 752 and 1 200 h, the weight gain rates are 0.099% and 0.26%, respectively. Wang et al.[25] prepared a HfB_2-SiC-Si/SiC coating using SiC whisker. The sample is pro-

Received date: 2020-03-19; **Revised date:** 2020-05-21

Corresponding author: XU Lei-hua, Associate Professor. E-mail: xuleihua@cumt.edu.cn

Author introduction: REN Xuan-ru, Associate Professor. E-mail: XuanruRen@163.com

tected by the HfB_2-SiC-Si/SiC coating, and the weight loss rate is only 0.88% after oxidation at 1500 °C for 468 h. Therefore, the HfB_2-SiC coating shows great potential for oxidation protection and has great advantages, However, the CO or CO_2 generated during the oxidation process of SiC will not only generate pores in the coating, but also easily cause the bubbling phenomenon of the self-produced glass film, and the pores or cracks will be generated in the glass layer after the bubbles break. These defects will increase the diffusion channel of oxygen to the matrix and weaken the oxidation protection ability of the composite glass layer. Therefore, in order to weaken the negative influence of gas by-products on the protection ability of the glass layer and improve the oxidation protection effect of the HfB_2-SiC coating, it is necessary to find a substitute of SiC component. However, due to its good oxygen resistance, especially its good thermal expansion matching with carbon matrix, SiC is irreplaceable. In this case, it is very attractive to modify the HfB_2-SiC coating by silicide with better oxygen resistance[26–29].

Among the silicide, $MoSi_2$ has high hardness, high oxidation resistance and corrosion resistance. In recent years, it has been widely used in the field of the anti-oxidation coating[30–36]. Zhang[37] et al. prepared a C/SiC/$MoSi_2$-Si multilayer anti-oxidation protective coating by combing a slurry method and gas-phase silicon penetration method, which can effectively protect carbon matrix for 300 and 103 h in 1 500 and 1 600 °C, respectively. Jiang[38] et al. prepared a SiC-Si/Mo-SiC-C coating by combing gas phase silicon infiltration technology and an impregnation method. The weight loss rate of the coating sample was only 0.96% when the sample was oxidized in air at 1 600 °C for 220 h. Li et al.[39] prepared a $MoSi_2$-SiC-Si anti-oxidation coating for protecting the C/C composite material by a two-step embedding method. The weight loss rate of the coating is only 1.04% after oxidation in air for 200 h at 1 500 °C. In addition, for $MoSi_2$ and SiC with the same amount, the amount of SiO_2 produced by $MoSi_2$ oxidation is twice that of SiC. In view of the sealing and oxygen blocking effect of SiO_2, more SiO_2 can effectively improve the overall sealing and oxygen blocking ability of the coating, weaken the oxidation loss of the coating, and thus reduce the generation of gas by-products. Therefore, it is very hopeful to improve the oxidation protection effect of the composite glass layer by modifying the HfB_2-SiC composite coating with $MoSi_2$.

In our previous study[40], we used Si, C, B_2O_3, HfO_2 and Mo powder as raw materials to prepare a HfB_2-$MoSi_2$-SiC anti-oxidation coating on the surface of the C/C composite with in-situ formed SiC as an inner coating layer. The weight loss of the coating matrix is only 0.76% after 408 h of isothermal static oxidation protection at 1 500 °C. However, it is difficult to precisely control the content and thickness of each component of the coating, and it is difficult to further study the effect of $MoSi_2$ modification on the oxygen resistance and protection mechanism of the HfB_2-SiC composite coating, which greatly limit its application.

In view of the potential of the HfB_2-$MoSi_2$-SiC coating prepared by high temperature reaction sintering technology in the construction of high oxygen resistance coating structure on a carbon substrate, we developed a liquid-phase sintering method by combining an in-situ reaction method with a slurry method, using HfB_2 powder, $MoSi_2$ powder, SiC powder, Si powder and C powder as raw materials and silica sol ($SiO_2 \cdot nH_2O$) as a binder to overcome the shortcomings on the control of coating component content and thickness. The HfB_2-$MoSi_2$-SiC coating with controllable composition, content and thickness was prepared by this method. The composition and content of the coating can be controlled by adjusting the slurry ratio, the coating thickness can be controlled by the brushing time, and the pressureless sintering can be realized by high temperature liquid phase reaction sintering at 2 100 °C. By adjusting the composition of the HfB_2-$MoSi_2$-SiC coatings, the effect of the $MoSi_2$ content on the oxygen resistance, oxidation protection behavior and oxidative protection mechanism of the HfB_2-SiC composite coating in the dynamic aerobic environment from room temperature to 1 500 °C and in the static constant temperature air at 1 500 °C were

studied, and the film-forming mechanism and oxygen resistance performance of the composite glass layer on the coating surface were analyzed.

2 Experimental

2.1 Sample preparation

In order to study the effect of the $MoSi_2$ content on the oxidative protection perfromance of the HfB_2-SiC coating, three kinds of HfB_2-$MoSi_2$-SiC coatings with $MoSi_2$ contents of 0, 20 wt.% and 40 wt.% were prepared. Firstly, the SiC inner coating layer was prepared on the surface of graphite matrix (Shanxi Xi'an Carbon Factory, 3 × 3 × 3 mm^3) by an embedding method with Si powder (Shanghai Jiuling smelting Co., Ltd, 3-5 μm, ⩾99.9%) and C powder (Shanxi Xi'an Carbon Factory, 2-3 μm, ⩾99.9%) as raw materials. The specific preparation process can be seen in our previous work[41]. Secondly, $MoSi_2$ powder (Hunan Zhuzhou Cemented Carbide Group Co., Ltd, 3-5 μm, ⩾99.9%), SiC powder (Beijing Zhongxin metal material technology Co., Ltd, 200 mesh, ⩾99.9%), Si powder, C powder and self-made HfB_2 powder[42] were used as raw materials, and silica sol ($SiO_2 \cdot nH_2O$) (Shandong Dezhou Jinghuo Technology Glass Co., 6-10 μm, 20 wt.%.) was used as a binder. The magnetic mixer was used to stir the raw material for 12 min at 80 °C at a rate of 600 r s^{-1} to obtain the mixed slurry. Then, the mixed slurry ($V_{\text{silica sol}}$: $M_{\text{other raw materials}}$=1 mL g^{-1}) was evenly brushed on the surface of graphite matrix with the SiC inner coating layer, and dried at 100 °C for 30 min, and this step was repeated three times after the slurry coating was completely dried. Finally, the sample was placed in a sintering furnace at 2 100 °C, and the sample was sintered under Ar gas atmosphere protection for 120 min to obtain the sample with a HfB_2-SiC-$MoSi_2$/SiC coating. The chemical reactions (Fig. 1) that occur during liquid phase sintering are as follows:

$$\mathrm{Si(s)+C(s)\rightarrow SiC(s)} \quad (1)$$

2.2 Material characterization

The crystal structure of the prepared HfB_2 powder and HfB_2-$MoSi_2$-SiC coating before and after oxidation was detected and analyzed using X-ray diffractometer (Bruker D8 ADVANCE XRD, Bruker AXS, Germany). The microstructure of HfB_2-$MoSi_2$-SiC coating before and after oxidation was studied by field emission scanning electron microscopy (JSM-6700F FE-SEM, JEOL, Japan). The crystal structure and microstructure of HfB_2 powder were detected by transmission electron microscopy (JEM-3010, TEM, JEOL, Japan). The dynamic oxidation protection performance of the HfB_2-$MoSi_2$-SiC coating was tested by thermogravimetry (STA 449 F3, TGA, Netzsch, Germany) from room temperature to 1 500 °C. In addition, a static constant temperature oxidation test of the coating at 1 500 °C was conducted in a high-temperature resistance furnace (M4/18AE, SGM, China).

3 Results and discussion

3.1 Analysis of phase and microstructure of the coating

Fig. 2a shows the TEM image of HfB_2 powder. As can be seen from Fig. 2a, the size of HfB_2 crystal is in the range of about 40-320 nm. In order to further

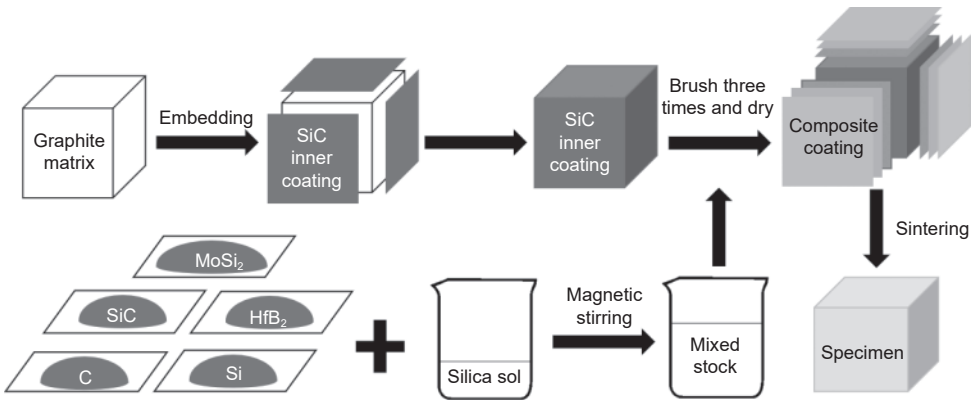

Fig. 1　Synthesis diagram of the HfB_2-SiC-$MoSi_2$/SiC coating prepared by a liquid phase sintering method.

study the microstructure of HfB_2 powder, the high resolution TEM image is shown in Fig. 2b. Clear lattice fringes can be observed in Fig. 2b, and the distances between crystal faces are about 0.273 and 0.214 nm, which are consistent with the (100) and (101) crystal faces of the HfB_2 PDF standard card (01-089-3651), indicating HfB_2 powder has a good crystallinity.

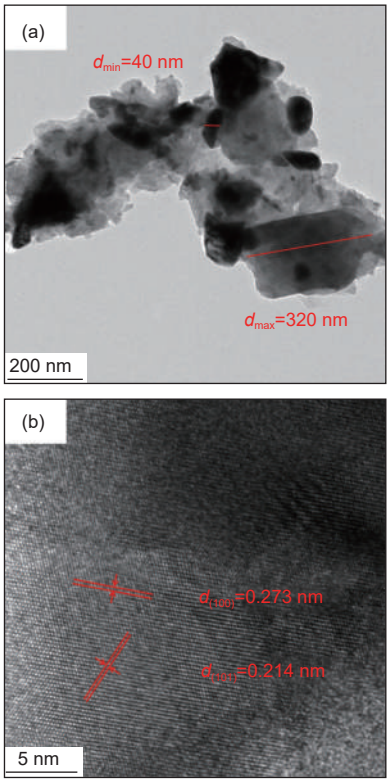

Fig. 2 TEM images of HfB_2 powder.

In order to study the phase composition of the HfB_2-$MoSi_2$-SiC composite coating, XRD pattern is shown in Fig. 3. As can be seen from Fig. 3, the coating is composed of three phases of HfB_2, SiC and $MoSi_2$, and no by-products are generated in the preparation process, indicating the successful preparation of the HfB_2-$MoSi_2$-SiC composite coating.

In order to have a clearer understanding of the microstructure of the HfB_2-$MoSi_2$-SiC composite coating, the micro morphology of the sample surface is analyzed by backscatter SEM technology, as shown in Fig. 4. It can be seen that the surface of the HfB_2-$MoSi_2$-SiC composite coating is relatively dense, and there are no visible cracks and other defects. In addition, the dense coating is mainly composed of the

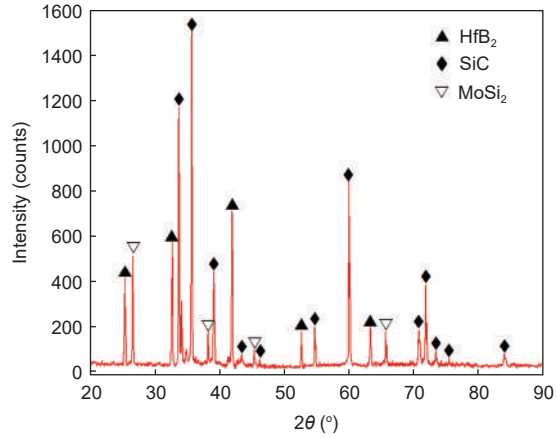

Fig. 3 XRD pattern of the HfB_2-$MoSi_2$-SiC coating.

phases with light gray, black and white three different colors. As shown in Fig. 4(b-d), the light gray phase in the area 1 is $MoSi_2$, the white phase in the area 2 is HfB_2, and the black phase in the area 3 is SiC, which are consistent with the XRD test results shown in Fig. 3.

Fig. 5 shows the cross-section backscatter SEM morphology of the SiC inner coating layer and the HfB_2-$MoSi_2$-SiC/SiC composite coating. It can be seen from Fig. 5a that the inner coating thickness of pure SiC is about 60-80 μm, and it is well bonded with carbon matrix. After the outer coating layer is prepared on the surface, as shown in Fig. 5b, the area A is the HfB_2-$MoSi_2$-SiC coating, the area B is SiC inner coating and the area C is graphite matrix. The thickness of the coating is about 120-150 μm. There is no obvious boundary between the inner and outer layers. This is because during the preparation of the outer layer, the liquid silica sol slurry carries HfB_2 powder, $MoSi_2$ powder, SiC powder, Si powder, C powder and other raw materials into the inner coating through the pores of the inner coating layer, and then in the process of liquid-phase sintering, SiC is generated through the solid-phase reaction between Si powder and C powder.

Thus, a form of mechanical occlusion and chemical combination is formed between the inner and outer layers, which improves the binding force between the inner and outer layers. In addition, the HfB_2-$MoSi_2$-SiC/SiC composite coating does not show obvious holes and cracks, which reflects the good thermal expansion coefficient matching between the

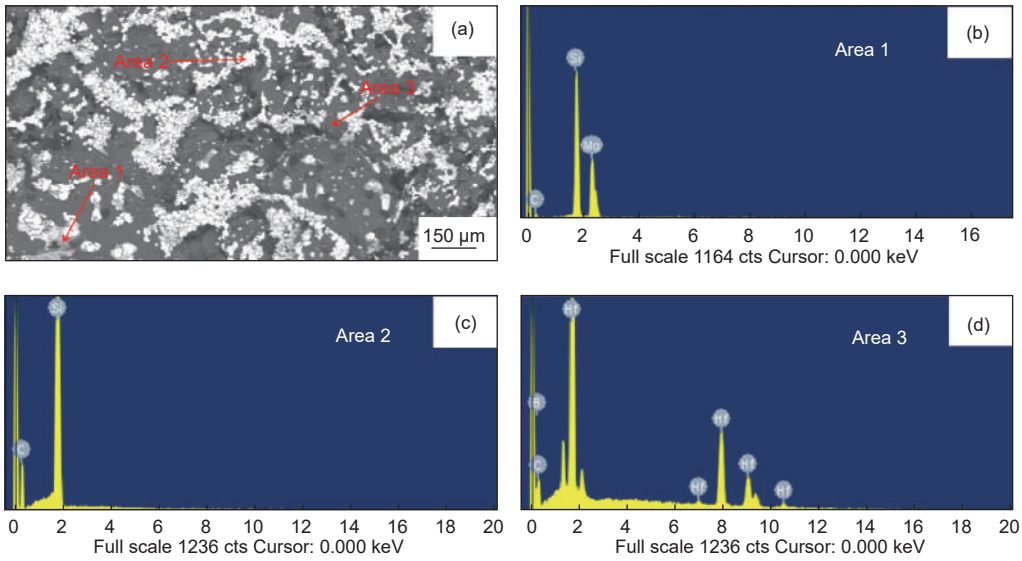

Fig. 4　SEM images and EDS of the HfB_2-$MoSi_2$-SiC composite coating.

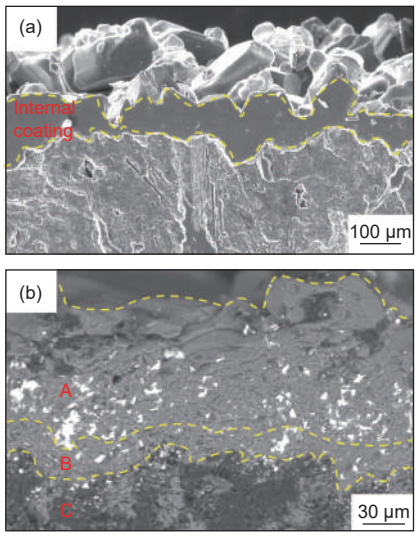

Fig. 5　Section backscattering SEM images of (a) the SiC inner coating layer and (b) the HfB_2-$MoSi_2$-SiC/SiC composite coating.

coating and the substrate, indicating that the liquid-phase sintering process effectively promotes the integration of the inner layer and the outer layer.

3.2　Study on the oxidative protection performance of the coatings

Fig. 6 shows the TG curves of the HfB_2-$MoSi_2$-SiC composite coatings from room temperature to 1 500 °C in air. It can be seen from the figure that the quality of the three composite coatings does not change significantly from room temperature to 700 °C, which indicates that these coatings have good oxidation protection ability below 700 °C. When the temperature is over 700 °C, the weight of all the coating samples shows the trend of a first increase and then decrease. The difference is that the temperature at which the sample begins to lose weight is different. The HfB_2-SiC coatings containing 0, 20 wt.% and 40 wt.% $MoSi_2$ have initial weight loss temperatures of 775, 808 and 821 °C, respectively.

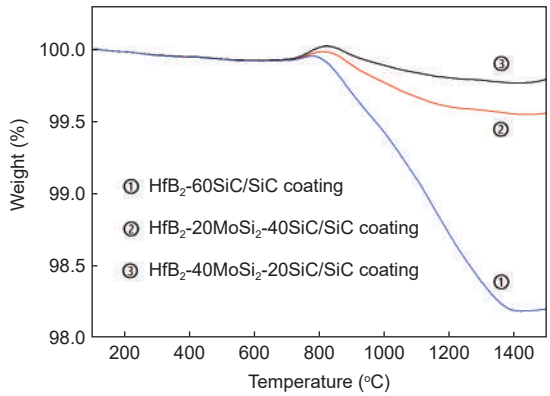

Fig. 6　TG curves of the HfB_2-$MoSi_2$-SiC composite coatings from room temperature to 1 500 ℃ in air.

Therefore, compared with the HfB_2-60SiC coating, the initial oxidation temperatures of the HfB_2-20$MoSi_2$-40SiC coating and HfB_2-40$MoSi_2$-20SiC coating are delayed by 4.2% and 5.9%, respectively, indicating the improvement the protective ability of the coatings containing $MoSi_2$ in the middle temperature range. In addition, at the end of TG test, the weight loss rate of the HfB_2-60SiC composite coating on the surface is 1.8%, while the final weight loss rates of the samples with 20 wt.% and 40 wt.%. $MoSi_2$

are only 0.45% and 0.21%, 75% and 88% lower than the sample without $MoSi_2$, respectively, indicating that the addition of $MoSi_2$ significantly improves the oxidation protection ability of the samples in wide temperature range.

In addition, it can be seen from Fig. 6 that although the curves of all coating samples show the state of weight loss when the temperature is higher than 850 °C, the downward shift trend of the samples with $MoSi_2$ becomes more slow as the temperature increases. In order to further study the oxidation protection mechanism of the composite coating, the weight loss rate curves of the HfB_2-$MoSi_2$-SiC composite coating samples are calculated according to formula (2), as shown in Fig. 7. The weight loss rate of all samples increase rapidly, and almost reach the maximum weight loss rate near 1 000 °C. Under the protection of HfB_2-60SiC coating, the maximum weight loss rate of the samples is 0.9×10^{-3} mg·cm^{-2}·s^{-1}. After adding 20 wt.% and 40 wt.% of $MoSi_2$, the maximum weight loss rates of the samples are 0.36×10^{-3} and 0.2×10^{-3} mg·cm^{-2}·s^{-1}, 60% and 78% lower than the sample without $MoSi_2$, respectively. In addition, there is an obvious fastest weight-loss temperature region in the temperature range of 1 000-1 200 °C, but after adding 20 wt.% and 40 wt.% of $MoSi_2$, there is almost no fastest weight-loss temperature region after the maximum weight-loss rate is reached. Therefore, the addition of $MoSi_2$ can effectively inhibit the maximum weight-loss rate and the fastest weight-loss area in the wide temperature range. The narrow fastest weight loss temperature region and low maximum weight loss rate will delay the oxidation process of the coating and reduce the risk of carbon matrix failure, thereby improving the oxidation protection ability of the coating in a wide temperature range.

$$V = \frac{\Delta m}{\Delta t \times s} \times 100\% \tag{2}$$

Where V is the weight loss rate of the coating, Δm (g) is the weight change of the sample to be tested, s (cm^2) is the surface area of the sample to be tested and Δt (s) is the unit time of sample oxidation to be tested.

Since the penetration of oxygen through the coating into the substrate is the main reason for the oxidation loss of the carbon substrate, we propose a calculation method of the relative oxygen permeability, as shown in formula (3), by which the influence of the addition of $MoSi_2$ on the relative oxygen permeability of the coating is further studied. The mass loss of the sample can be used as the measurement of oxygen permeability. Firstly, we choose the HfB_2-60SiC coating as the standard sample, and set the mass loss per unit area as a benchmark of the oxygen permeability. Secondly, the ratio of mass loss per unit area between the sample to be tested and the reference sample is taken as the relative oxygen permeability. Finally, according to formula (3), the relative oxygen permeabilities of the coatings containing $MoSi_2$ are shown in Fig. 8.

$$RP_{O_2} = \frac{\Delta m_1 \times s_0}{\Delta m_0 \times s_1} \times 100\% \tag{3}$$

RP_{O_2} is the relative oxygen permeability of the coating, Δm_1 (g) is the weight change in unit time of

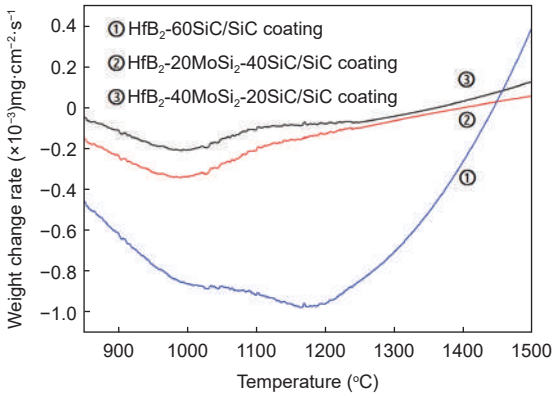

Fig. 7 Weight loss rate curves of three HfB_2-$MoSi_2$-SiC composite coatings.

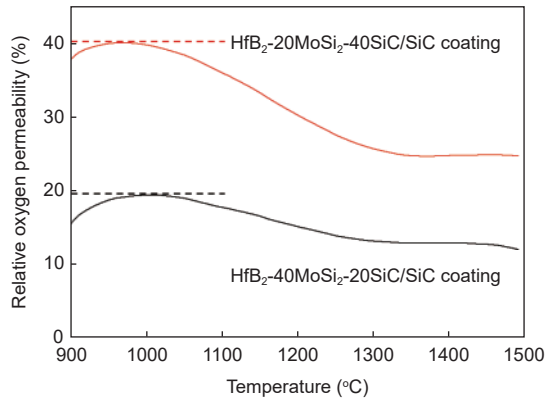

Fig. 8 Relative oxygen permeability curves of the HfB_2-$MoSi_2$-SiC composite coatings containing $MoSi_2$.

the sample to be tested, Δm_0 (g) is the weight change in unit time of the sample to be tested, S_1 (cm^2) is the surface area of the sample after oxidation in unit time of the sample to be tested, and S_0 (cm^2) is the surface area of the sample after oxidation in unit time of the sample to be tested. The lower the RP_{O_2} value, the better the oxygen resistance of the coating.

It can be seen from Fig. 8 that after adding 20 wt.% and 40 wt.% of $MoSi_2$ into the coating, the maximum relative oxygen permeabilities of the HfB_2-$MoSi_2$-SiC coatings are 40.1% and 19.4%, respectively. That is to say, compared with the HfB_2-SiC coating, the HfB_2-20$MoSi_2$-40SiC coating and HfB_2-40$MoSi_2$-20SiC coating block 59.9% and 80.6% oxygen diffusion to the substrate at most. In addition, with the increase of temperature, the relative oxygen permeabilities of the coating decrease, indicating that the oxygen resistances of the coatings increase with the increase of temperature. At about 1 300 °C, the relative oxygen permeabilities of the coatings tend to be stable because the silicate glass layers formed by oxidation begin to play a role gradually. The minimum relative oxygen permeabilities of the coating containing 20 wt.% and 40 wt.% of $MoSi_2$ are 24.7% and 12.2%, respectively. It can be seen that the addition of $MoSi_2$ can effectively reduce the oxygen permeability of the coating, thus reducing the oxidation corrosion of oxygen on the substrate and improving the oxidation protection ability of the coatings in a wide temperature range.

In order to further study the high temperature stability and oxidation protection ability of the coatings. Fig. 9 shows the isothermal oxidation curves of the HfB_2-$MoSi_2$-SiC composite coatings oxidized for 200 h at 1 500 °C in air. In the early stage of oxidation, the coatings are in full contact with oxygen, and chemical reactions (4-7) take place, resulting in the phenomenon of weight gain of the initial samples. Subsequently, the amount of SiO_2 glass formation increases gradually, and due to its good sealing effect, the oxidation of the coatings are obviously inhibited, so the samples do not show the phenomenon of weight gain continuously. In addition, the coatings began to lose weight after 40 h of oxidation, which indicates that the coatings could not completely block the oxygen permeation, and oxygen diffusion channels exist. When the coating iss oxidized at a constant temperature for 200 h, the weight loss ratio of the sample protected by the HfB_2-SiC coating is 0.46%, while the weight loss rate of the samples protected by the HfB_2-20$MoSi_2$-40SiC coating and HfB_2-40$MoSi_2$-20SiC coating are 0.27% and 0.08%, 41.3% and 79.2% lower than the sample without $MoSi_2$, respectively. The results show that the high temperature oxidation protection stability of the coatings is significantly improved due to the replacement of a part of SiC in the coating by $MoSi_2$, thus providing more reliable oxidation protection for carbon matrix.

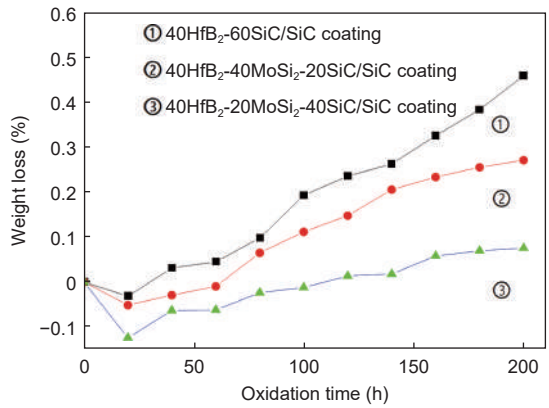

Fig. 9　Isothermal oxidation curves of HfB_2-$MoSi_2$-SiC coatings at 1 500 ℃.

In order to further study the phase composition of the coatings after oxidation, the XRD patterns of HfB_2-$MoSi_2$-SiC composite coatings after static oxidation for 200 h at 1 500 °C in air are shown in Fig. 10. It can be seen that after oxidation, all the coatings contain SiC, SiO_2, HfO_2 and $HfSiO_4$ phases, indicating that a composite glass layer is formed on the surface of the coating. However, the diffraction peaks of B_2O_3 and MoO_3 are not detected in Fig. 10. On the one hand, the vaporization temperature of B_2O_3 is around 1 300 °C[43], while the boiling point of MoO_3 is 1 155 °C. The vaporization of B_2O_3 and MoO_3 at the oxidation test temperature results in the absence of two phases on the surface. On the other hand, B_2O_3 can react with SiO_2 to form borosilicate glass, further

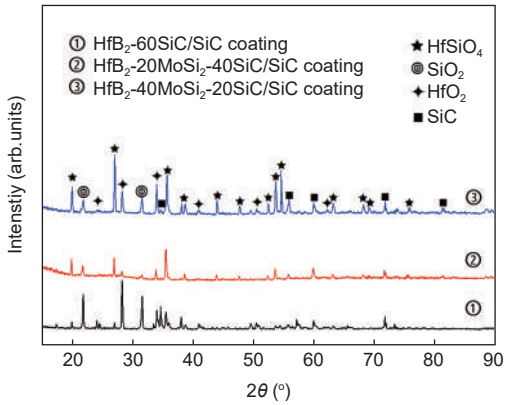

Fig. 10 XRD patterns of HfB_2-$MoSi_2$-SiC composite coatings after static constant temperature oxidation at 1 500 ℃ for 200 h.

weakening the diffraction peaks on the surface. As $HfSiO_4$ and HfO_2 are very stable at high temperature [44], the stability of SiO_2 glass layer can be improved with the formation of a Hf-Si-O glass layer, so their formation can improve the high temperature oxidation protection ability of the coatings. The chemical reaction equations during oxidation are as follows:

$$SiC(s) + 2O_2(g) \rightarrow SiO_2(s) + CO_2(g) \quad (4)$$

$$2SiC(s) + 3O_2(g) \rightarrow 2SiO_2(s) + 2CO(g) \quad (5)$$

$$2HfB_2(s) + 5O_2(g) \rightarrow 2HfO_2(s) + 2B_2O_3(s) \quad (6)$$

$$2MoSi_2(s) + 7O_2(g) \rightarrow 2MoO_3(g) + 4SiO_2(s) \quad (7)$$

$$SiO_2(s) + HfO_2(s) \rightarrow HfSiO_4(s) \quad (8)$$

$$SiC(s) + 2SiO_2(g) \rightarrow 3SiO(g) + CO(g) \quad (9)$$

$$B_2O_3(s) \rightarrow B_2O_3(l) \rightarrow B_2O_3(g) \quad (10)$$

$$C(s) + O_2(g) \rightarrow CO_2(g) \quad (11)$$

$$2C(s) + O_2(g) \rightarrow 2CO(g) \quad (12)$$

In order to further explore the surface microstructure of the coatings after oxidation, Fig. 11(a-c) shows the surface backscatter SEM morphology of the composite coatings containing HfB_2-$MoSi_2$-SiC after TG dynamic oxidation from room temperature to 1 500 °C. It can be seen that the coating surfaces are mainly composed of light gray and white areas. It can be seen from Fig. 11(d-e) that the white phase in Fig. 11a is Hf oxide, while the main elements of light gray phase in the area 2 are Si and O, so the gray phase is SiO_2, which is consistent with the XRD test results shown in Fig. 10. In addition, it can be seen from Fig. 11a that the oxides of Hf are mainly dis-

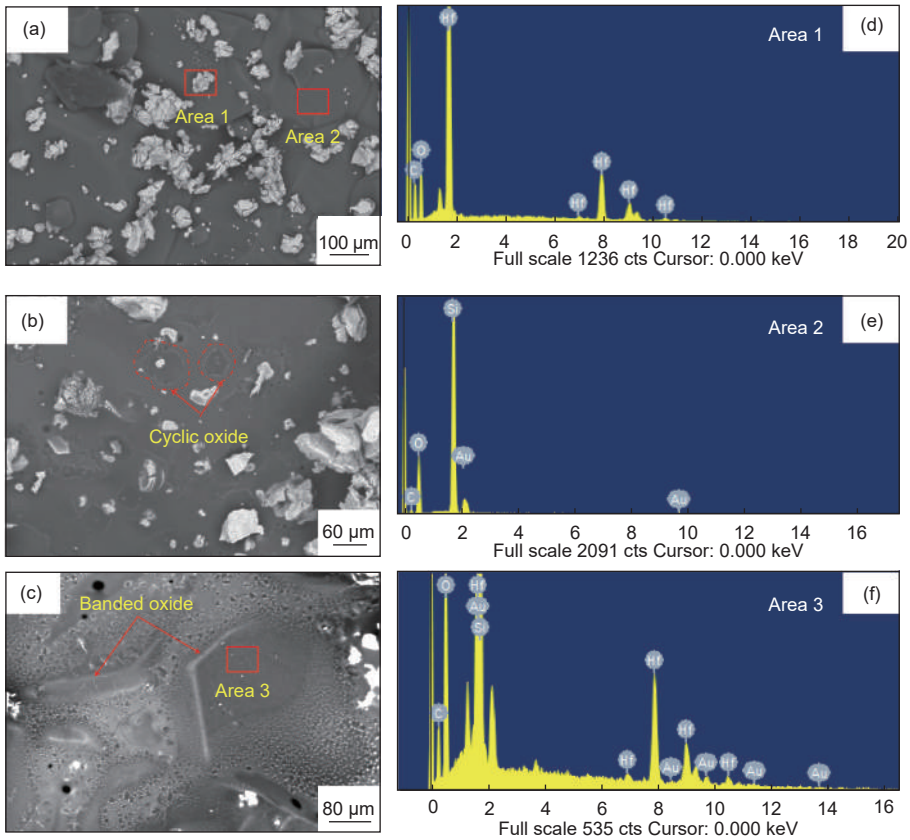

Fig. 11 SEM morphology and EDS of the HfB_2-$MoSi_2$-SiC coatings after dynamic oxidation at room temperature to 1 500 ℃: (a)HfB_2-60SiC, (b)HfB_2-20$MoSi_2$-40SiC, (c)HfB_2-40$MoSi_2$-20SiC, (d) EDS of the region 1, (e) EDS of the region 2 and (f) EDS of the region 3.

persed on the surface of the coating with large particles. It can be seen from Fig. 11(b-c) that with the increase of the $MoSi_2$ content, there is a ring of oxide dispersion around the large particles of Hf oxide. With the increase of the $MoSi_2$ conten in the composite coatings, the dispersion of the oxide becomes more and more obvious. This is because with the increase of the amount of SiO_2 glass phase on the surface of the coating, the flow of SiO_2 glass phase is intensified, and the strength of Hf oxide dispersed on the surface of the coatings is increased, so as to accelerate the homogeneous distribution of Hf oxide on the surface of the coatings. EDS analysis of Fig. 11f shows that the main elements in the light gray phase area 3 of Fig. 11c are Hf, Si and O. Due to the dispersion of Hf oxide, the glass layer on the coating surface becomes a Hf-Si-O composite glass layer.

In order to further study the anti-oxidation protection mechanism of the composite glass layers in long-term service at high temperature, Fig. 12(a-c) shows the surface backscatter SEM morphology of the composite coatings containing HfB_2-$MoSi_2$-SiC after static constant temperature oxidation for 200 h at 1 500 °C.

It can be seen from Fig. 12(a-c) that after full oxidation, the glass layers of the coatings have completely covered by the coating surface. Because of the poor matching of the thermal expansion coefficient, cracks can be observed in the glass film when the samples are cooled to room temperature. Although these cracks will be self-healed by the flow dynamic glass layer at high temperature in the alternative environment of high and low temperature. When the cracks are not healed, these cracks will be used as the diffusion channel of oxygen, resulting in the oxidation loss of carbon matrix. Therefore, the less the number of cracks in the glass layer, the better the oxidation protection effect. With the increase of the $MoSi_2$ content, the dispersion of Hf oxide on the surface of Hf-Si-O composite glass layer is intensified, and the cracks in the coating become less and less, which shows that the Hf-Si-O composite glass layer has excellent stability, showing the mechanism of Hf oxide dispersion enhancement of the coating stability.

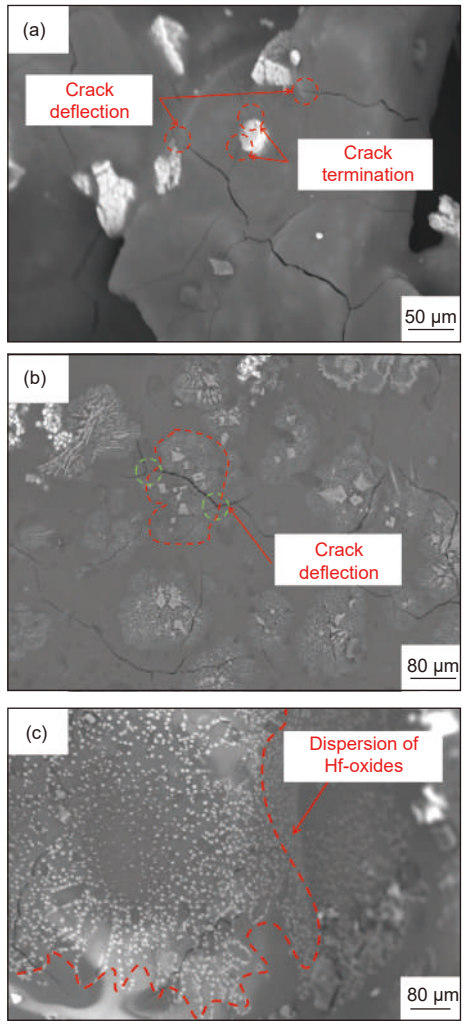

Fig. 12　SEM images of surface backscatter of HfB_2-$MoSi_2$-SiC coatings after static constant temperature oxidation at 1 500 ℃ for 200 h: (a)HfB_2-60SiC, (b)HfB_2-20$MoSi_2$-40SiC and (c)HfB_2-40$MoSi_2$-20SiC.

In addition, it can be seen from Fig. 12(a-c) that the cracks mainly exist in the region with less Hf oxide (black region). At the same time, the deflection and termination of the cracks can be clearly observed around the oxides of large white particles Hf in the glass layer, which indicates that when the oxide layer changes to glass state, the large Hf oxide particles are embedded in the glass layer in the form of "pinning phase", which limits the crack growth to a certain extent, thus reducing the number of the oxygen diffusion channels in the glass layer and reducing the glass layer oxygen permeation during the transition from glassy state to molten state, which further increases the oxidation protection of Hf-Si-O composite glass

layer on carbon matrix.

4 Conclusions

HfB_2-$MoSi_2$-SiC composite coatings were successfully prepared by a liquid phase sintering method. The surface of the coatings is compact, and there are no visible cracks, holes and other defects. It is proved that the coatings have good thermal expansion coefficient matching with the matrix. The results of dynamic oxidation test from room temperature to 1 500 °C show that with the increase of the $MoSi_2$ content, the initial oxidation temperatures of the samples are delayed from 775 to 821 °C, and the maximum weight loss rate is reduced from 0.9×10^{-3} to 0.2×10^{-3} $mg\cdot cm^{-2}\cdot s^{-1}$, the fastest weight loss temperature area is narrowed, and the lowest relative oxygen permeability is reduced to 12.2%, which makes the weight loss rate of the samples reduce from 1.8% to 0.21%, improving the oxidation protection ability of the coatings in the wide temperature range. The results of static isothermal oxidation test at 1 500 °C show that the increase of the $MoSi_2$ content can increase the formation of SiO_2 glass phase in the coating, promote the dispersion of Hf oxide on the coating surface, and form a Hf-Si-O composite glass layer with higher stability and self-healing ability. The composite phase glass layers can effectively inhibit the crack formation, force the crack termination or deflection, thus reducing the weight loss rate of the samples after static constant temperature oxidation at 1 500 °C from 0.46% to 0.08%, significantly enhancing the high temperature stability of the coating, and providing reliable oxidation protection for the carbon matrix.

Acknowledgements

The Fundamental Research Funds for the Central Universities (2018GF14).

References

[1] Li H J, Chen M M, Yao X Y, et al. Status and prospect of self-healing for carbon/carbon composites research[J]. Journal of the Chinese Ceramic Society, 2018, 46(01): 142-149.

[2] Silvestroni L, Guicciardi S, Melandri C, et al. TaB_2-based ceramics: Microstructure, mechanical properties and oxidation resistance[J]. Journal of the European Ceramic Society, 2012, 32: 97-105.

[3] Huang M, Li K Z, Li H J, et al. Yttrium silicate coatings for SiC coated C/C composites prepared by atmospheric plasma spraying[J]. New Carbon Materials, 2010, 25(3): 187-191.

[4] Silvestroni L, Bellosi A, Melandri C, et al. Microstructure and properties of HfC and TaC-based ceramics obtained by ultrafifine powder[J]. Journal of the European Ceramic Society, 2011, 31: 619-27.

[5] Liu Y, Fu Q G, Zhao F L, et al. Internal friction vs. thermal shock in C/C composites[J]. Part B-Engineering, 2016, 106: 59-65.

[6] Zhang Y L, Hu H, Zhang P F, et al. SiC/ZrB_2-SiC-ZrC multilayer coating for carbon/carbon composites against ablation[J]. Surface & Coatings Technology, 2016, 300: 1-9.

[7] Corral E, Walker L. Improved ablation resistance of C-C composites using zirconium diboride and boron carbide[J]. Journal of the European Ceramic Society, 2010, 30: 2357-2364.

[8] Liu T Y, Fu Q G, Cheng C Y. Effects of particle impacting on ablation property of C/C-ZrC-SiC composites via injection method[J]. Equipment Environmental Engineering, 2019, 16(10): 8-15.

[9] Zhou L, Huang J F, Cao L Y, et al. A novel design of oxidation protective β-$Y_2Si_2O_7$ nanowire toughened Y_2SiO_5/Y_2O_3-Al_2O_3-SiO_2 glass ceramic coating for SiC coated carbon/carbon composites[J]. Corrosion Science, 2018(135): 233-242.

[10] Li H J, Shi X H, Shen Q Q, et al. Research and development of C/C composites in China[J]. The Chinese Journal of Nonferrous Metals, 2019, 29(9): 2142-2154.

[11] Jortenr J, Priya N S. Applications of carbon/carbon composites[J]. Comprehensive Composite Materials II, 2018, 5: 421-436.

[12] Peng Z, Sun W, Xiong X, et al. Microstructure characteristics and ablation behavior of an $Al_{1.92}Cr_{0.08}O_3$-SiC-ZrC anti-ablation coating[J]. New Carbon Materials, 2019, 34(5): 464-471.

[13] Mi Q, Cao L Y, Huang J Q F, et al. Research progress in matrix oxidation-resistance modification of carbon/carbon composites[J]. Ordnance Material Science and Engineering, 2010, 33(02): 98-103.

[14] Dietrich S, Gebert J M, Stasiuk G, et al. Microstructure characterization of CVI-densified carbon/carbon composites with various fiber distributions[J]. Composites Science Technology, 2012(72): 1892-1900.

[15] Zhang J P, Fu Q G, Qu J L, et al. Blasting treatment and chemical vapor deposition of SiC nanowires to enhance the thermal shock resistance of SiC coating for carbon/carbon composites in combustion environment[J]. Journal of Alloys and Compounds, 2016(666): 77-83.

[16] Li Z Q, Li H J, Cao C W, et al. Investigation on ablation characteristics of C/C composites with ZrC/SiC coating[J]. Journal of Solid Rocket Technology, 2011, 34(1): 105-108.

[17] Li S P, Zhang M Y, Huang D, et al. Preparation and antioxidation property of a SiC-$MoSi_2$-Si multilayer coating on a C/C composite[J]. New Carbon Materials, 2018, 33(1): 82-87.

[18] Venugopal S, Paul A, Vaidhyanathan B, et al. Synthesis and spark

plasma sintering of submicron HfB_2: Effect of various carbon sources[J]. Journal of the European Ceramic Society, 2014(34): 1471-1479.

[19] Silvestroni L, Sciti D. Densification of ZrB_2-$TaSi_2$ and HfB_2-$TaSi_2$ ultra-high-temperature ceramic composites[J]. Journal of the American Ceramic Society, 2011(94): 1920-1930.

[20] Talmy I G, Zaykoski J A, Opeka M M. Synthesis, processing and properties of TaC-TaB_2-C ceramics[J]. Journal of the European Ceramic Society, 2010(30): 2253-2256.

[21] Ren J C, Zhang Y L, Zhang P F, et al. Ablation resistance of HfC coating reinforced by HfC nanowires in cyclic ablation environment[J]. Journal of the European Ceramic Society, 2017(37): 2759-2768.

[22] Ren X R, Li H J, Chu Y H, et al. Ultra-high temperature ceramic HfB_2-SiC coating for oxidation protection of SiC-coated carbon/carbon composites[J]. International Journal of Applied Ceramic Technology, 2015, 12(3): 560-567.

[23] Wang P P, Li H J, Yuan R M, et al. The oxidation resistance of two-temperature synthetic HfB_2-SiC coating for the SiC coated C/C composites[J]. Journal of Alloys and Compounds, 2018, 747: 438-446.

[24] Jiang Y, Liu T Y, Ru H Q, et al. Oxidation and ablation protection of double layer HfB_2-SiC-Si/SiC-Si coating for graphite materials[J]. Journal of Alloys and Compounds, 2019, 782: 761-771.

[25] Wang T Y, Luo R Y. Oxidation protection and mechanism of the HfB_2-SiC-Si/SiC coatings modified by in-situ strengthening of SiC whiskers for C/C composites[J]. Ceramics International, 2018, 44(11): 12370-12380.

[26] Simonenko E P, Simonenko N P, Gordeev A N, et al. Behavior of HfB_2-30vol% SiC UHTC obtained by sol-gel approach in the supersonic airflow[J]. Journal of Sol-Gel Science and Technology, 2019, 92(2): 386-397.

[27] Wang P P, Li H J, Kong J A, et al. A WSi_2-HfB_2-SiC coating for ultralong-time anti-oxidation at 1973K[J]. Corrosion Science, 2019, 159: 108-119.

[28] Zhang J P, Fu Q G, Tong M D, et al. Microstructure, ablation behavior and thermal retardant ability of C/C-HfB_2 composites prepared by precursor infiltration pyrolysis combined with chemical vapor infiltration[J]. Journal of Alloys and Compounds, 2018, 742: 123-129.

[29] Zhang J P, Qu J L, Fu Q G, et al. Ablation behavior of nose-shaped HfB_2-SiC modified carbon/carbon composites exposed to oxyacetylene torch[J]. Corrosion Science, 2019, 151: 87-96.

[30] Sun J, Fu Q G, Guo L P, et al. Effect of filler on the oxidation protective ability of $MoSi_2$ coating for Mo substrate by halide activated pack cementation[J]. Materials & Design, 2016(92): 602-609.

[31] Wang L X, Fu Q G, Zhao F L. Improving oxidation resistance of $MoSi_2$ coating by reinforced with Al_2O_3 whiskers[J]. Intermetallics, 2018(940): 106-113.

[32] Fu Q Gg, Xue H, Li H J, et al. Anti-oxidation property of a multi-layer coating for carbon/carbon composites in a wind tunnel at 1500 °C[J]. New Carbon Materials, 2010, 25(4): 279-284.

[33] Zhang Y L, Li H J, Hu Z X, et al. C/SiC/$MoSi_2$-SiC-Si multilayer coating for oxidation protection of carbon/carbon composites[J]. Transactions of Nonferrous Metals Society of China, 2013(7): 2118-2122.

[34] Zhu L, Zhu Y S, Ren X R, et al. Microstructure, properties and oxidation behavior of $MoSi_2$-MoB-ZrO_2 coating for Mo substrate using spark plasma sintering[J]. Surface & Coatings Technology, 2019, 375: 773.

[35] Chen P, Zhu L, Ren X R, et al. Preparation of oxidation protective $MoSi_2$-SiC coating on graphite using recycled waste $MoSi_2$ by one-step spark plasma sintering method[J]. Ceramics International, 2019: 22040-22046.

[36] Chen P, Zhu L, Ren X R, et al. Recycling Waste $MoSi_2$ Heating elements to fabricated $MoSi_2$-based anti-oxidation coatings[J]. Equipment Environmental Engineering, 2019, 16(10): 55-58.

[37] Zhang Y L, Li H J, Hu Z X, et al. C/SiC/$MoSi_2$-SiC-Si multilayer coating for oxidation protection of carbon/carbon composites[J]. Transactions of Nonferrous Metals Society of China, 2013, 23: 2118-2122.

[38] Jiang Y, Ye C C, Ru H Q, et al. Oxidation protective $MoSi_2$-SiC-Si coating for graphite materials prepared by slurry dipping and vapor silicon infiltration[J]. Ceramics International, 2018, 44: 5171-5178.

[39] Li H J, Xue H, Wang Y J, et al. A $MoSi_2$-SiC-Si oxidation protective coating for carbon/carbon composites[J]. Surface and Coatings Technology, 2007, 201: 9444-9447.

[40] Wang P P, Li H J, Ren X R, et al. HfB_2-SiC-$MoSi_2$ oxidation resistance coating fabricated through in-situ synthesis for SiC coated C/C composites[J]. Journal of Alloys and Compounds, 2017, 722: 69-76.

[41] Ren X R, Li H J, Fu Q G, et al. TaB_2-SiC-Si multiphase oxidation protective coating for SiC-coated carbon/carbon composites[J]. Journal of the European Ceramic Society, 2013(15-16): 2953-2959.

[42] Yao D J, Li H J, Liu L, et al. HfB_2 prepared by sol-gel method and its oxidation behavior[J]. Rare Metal Materials and Engineering, 2013, 42(12): 2594-2597.

[43] Silvestroni L, Meriggi G, Sciti D, et al. Oxidation behavior of ZrB_2 composites doped with various transition metal silicides[J]. Corrosion Science, 2014, 83: 281-291.

[44] Wang P P, Li H J, Sun J, et al. The effect of HfB_2 content on the oxidation and thermal shock resistance of SiC coating[J]. Surface and Coatings Technology, 2018, 339: 124-131.